Mechanics & Industry **24**, 29 (2023)

https://doi.org/10.1051/meca/2023028

Mechanics & Industry

Available online at:
www.mechanics-industry.org

History of matter: from its raw state to its end of life
Prof. Amine Ammar (Guest Editor)

REGULAR ARTICLE

OPEN ACCESS

Mechanical modeling of growth applied to *Saccharomyces cerevisiae* yeast cells

Zeinab Awada[1,*], and Boumediene Nedjar[2]

[1] Sorbonne Université, Institut Jean Le Rond d'Alembert, CNRS, UMR 7190
[2] Université Gustave Eiffel, MAST/EMGCU

Received: 11 December 2022 / Accepted: 25 July 2023

Abstract. A theoretical and numerical model is developed to describe the growth of *Saccharomyces cerevisiae* yeasts. This kind of cells is considered here as an axisymmetrical and deformable structure, the inner surface of which is continuously acted upon by a high turgor pressure. Due to the small ratio between the cell-wall thickness and the cell radius, a structural shell approach is used. Moreover, the finite strain range is assumed because of the soft nature of these cells. The adopted kinematics is herein based on the multiplicative decomposition of the deformation gradient into an elastic part $\boldsymbol{F}^{\mathrm{e}}$ and an irreversible part related to the growth $\boldsymbol{F}^{\mathrm{g}}$, i.e. $\boldsymbol{F} = \boldsymbol{F}^{\mathrm{e}}\boldsymbol{F}^{\mathrm{g}}$. The reversible response is described using an hyperelastic model of the Ogden type. In accordance with continuum thermodynamics requirements, a criterion is introduced to control the evolution of the growth phenomenon. In this latter two parameters are involved: a growth stress-like threshold, and a growth characteristic time. Embedded within the finite element framework, an illustrative example shows the growth phenomenon of spherical cells going from yeast bud emergence to the step just before cell division. A parametric study highlights the influence of the above mentioned parameters on the cell responses.

Keywords: Growth / large deformation / *Saccharomyces cerevisiae* yeast / cell-wall / Turgor pressure

1 Introduction

Every living organism is made up at the base of an element that can be though as a mini-factory, called cell. In the cell biology field, there exist a large diversity of items that share many commun functions and architecture. *Saccharomyces cerevisiae* yeast provides a powerful system to study eukaryotic cells. It is easily manipulated in laboratory and it grows very quickly. Due to these features, in addition to the advantage of being regarded as safe, this yeast remains the host cell to investigate humain processes. In particular, *S. cerevisiae* yeast is known by its more common names, baker's yeast or brewer's yeast. It is widely used in food industry for baking, winemaking and brewing [1,2]. This yeast is also beneficial in the medical sector. It serves for the production of insulin and vitamins [3]. Moreover, yeast extracts help to improve skin health, see [4].

This yeast, as other fungal, bacterial and plant cells, are characterized by a high internal pression, called turgor pressure, [5]. It results from the pressure difference between the interior and the exterior of the cell. Over and above that, these species are surrounded by a tough and flexible structure; the cell-wall. The structure and composition of this latter are constantly adapted to accompany the permanent remodeling of cell architecture and the environmental changes. For example, a cell-wall expansion occurs simultaneously with the growth of the cell. The growth phenomenon corresponds to a replication of the content, increases of the total mass of the cell and it leads under ideal conditions to cell division.

In this work, we focus on the growth process of the *S. cerevisiae* yeast that poliferates by budding. During a cell cycle, only one bud can be formed at a time, giving rise to a cell daughter after division. The growth procedure could be stimulated by biological, chemical or mechanical factors, among others. Biological and biochemical stimulated growth have been previously studied. The variation of the cell-wall composition during growth has also been investigated. According to [6], at the base of the emerging bud, a chitin is formed.

Several studies have been conducted on growth driven by the turgor pressure. In [7], Basu et al. explored the role of this pressure in the fission of *Schizosaccharomyces pombe* yeast, while Rojas et al. worked on bacteries, see

* e-mail: zeinab.awada@sorbonne-universite.fr

[8]. Over the same period, two dynamic models have been developed on *S. cerevisiae* growth under turgor pressure, see [9]. These authors assumed that the yeast is a shell structure with an external radius of 2.5 µm and a wall thickness of 115 nm. They also hypothesized that the shell is pressurized by a turgor pressure estimated to 0.2 MPa. Furthermore, a mechanical feedback on the relation between cell-wall expansion and assembly is achieved in [10]. The budding yeast was assumed as a shell with a wall thickness ∼100 nm, very small with respect to the bud diameter ∼1 µm. In the present work, the emphasis will be on the purely mechanical aspects. The growth is stimulated by the stress state as a result of turgor pressure. Once the wall is acted upon this pressure, in-plane mechanical tensions will be created and lead to the cell-wall expansion.

The remainder of this contribution is as follow: in Section 2, we provide a summary of the quasi-Kirchhoff structural shell theory in the finite strain range together with the kinematic choice based on the multiplicative decomposition of the deformation gradient into reversible and growth parts. Later on, constitutive equations for the hyperelastic energy and the evolution equation of growth are given in accordance with continuum thermodynamic requirements. Section 3 is devoted to numerical simulations where a representative numerical example is shown together with a parametric study of the perhaps most important parameters; the growth threshold and the growth characteristic time. We end this paper with conclusions and perspectives.

2 Basic equations

Yeasts can be regarded as thin-walled shell structures and, due to their soft nature, a formulation within the finite strain range is herein adopted. We first review the basic kinematics that we extend toward finite growth. We next derive the constitutive equations that will be used later on for numerical simulations.

2.1 Shell kinematics with growth

As a starting point, use is made of the quasi-Kirchhoff-type theory for thin shells of revolution that has been derived in [11]. Briefly, denoting by $\boldsymbol{E}$ the Green-Lagrange strain tensor[1], its non-zero components reduce to the meridional, E_1, the circumferential, E_2, and the transverse shear, E_{13}, that are valid for finite rotations together with large strains. They can be split into membrane (m), bending (b) and shear (s) parts as:

$$E_\gamma = E_\gamma^m + \xi E_\gamma^b \quad (\gamma = 1, 2), \qquad \text{and} \qquad E_{13} = E_{13}^s \tag{1}$$

[1] We recall the definition $\boldsymbol{E} = \frac{1}{2}\left\{\boldsymbol{F}^T\boldsymbol{F} - \boldsymbol{1}\right\}$ of the Green-Lagrange strain tensor, where $\boldsymbol{F}$ is the deformation gradient with principal values λ_i, $i = 1 \ldots 3$, and $\boldsymbol{1}$ is the second-order identity tensor.

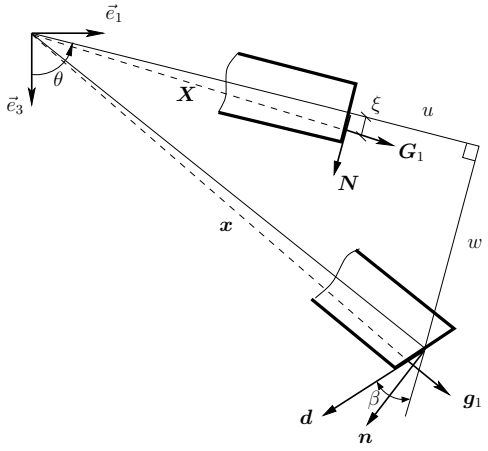

Fig. 1. Kinematics for geometrically nonlinear axisymmetric shells [12].

where ξ is the through-the-thickness coordinate. The different terms are given by, see [12] for full details,

$$\begin{aligned}
E_1^m &= u_{,s} + \frac{1}{2}(u_{,s}^2 + w_{,s}^2) \\
E_2^m &= e_\theta + \frac{1}{2}e_\theta^2 \\
E_1^b &= -[(1 + u_{,s})\cos\beta + w_{,s}\sin\beta]\beta_{,s} \\
E_2^b &= \frac{\cos\theta}{r} - rc_2(1 + e_\theta) \\
E_{13}^s &= -(1 + u_{,s})\sin\beta + w_{,s}\cos\beta
\end{aligned} \tag{2}$$

with the notations $r = s\sin\theta$, $e_\theta = (u\sin\theta - w\cos\theta)/r$, and $c_2 = (\sin\theta\sin\beta + \cos\theta\cos\beta)/r^2$, s being the arc length which represents the initial position. The displacement components u and w are relative to the local coordinate system, and β is the in-plane rotation angle of the director $\boldsymbol{d}$, see the sketch of Figure 1.

Next, as the shear strain E_{13} is set to zero by a penalty term, i.e. quasi-Kirchhoff shell theory, E_1 and E_2 are then regarded as principal strains. In this case, the principal stretches λ_i relative to the deformation gradient $\boldsymbol{F}$ follow from equation $(1)_1$ by considering the relation,

$$E_\gamma = \frac{1}{2}\left(\lambda_\gamma^2 - 1\right) \quad \Rightarrow \quad \lambda_\gamma = \sqrt{2E_\gamma + 1} \qquad \gamma = 1, 2 \tag{3}$$

together with $\lambda_3 = 1$.

Now for the extension toward finite growth, use is made in this work of the multiplicative decomposition of the deformation gradient into an elastic part $\boldsymbol{F}^{\mathrm{e}}$ and a growth part $\boldsymbol{F}^{\mathrm{g}}$ as proposed in [13], i.e. the sketch of Figure 2, see also [14,15],

$$\boldsymbol{F} = \boldsymbol{F}^{\mathrm{e}}\boldsymbol{F}^{\mathrm{g}}. \tag{4}$$

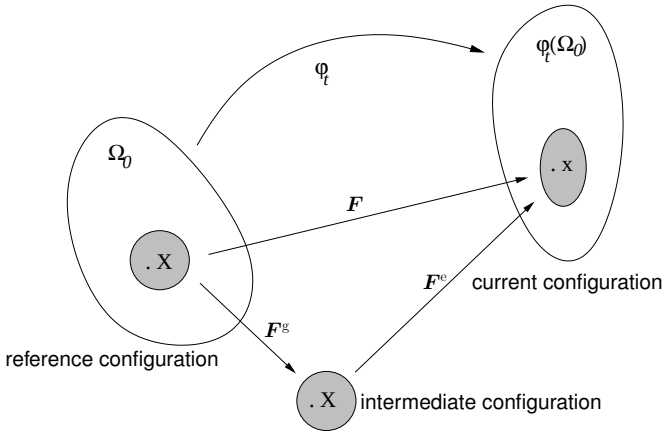

Fig. 2. Local decomposition of the deformation gradient for finite growth $\boldsymbol{F} = \boldsymbol{F}^{\mathrm{e}}\boldsymbol{F}^{\mathrm{g}}$.

From equation (4), a multiplivative decomposition of the stretches is then deduced,

$$\lambda_i = \lambda_i^{\mathrm{e}}\lambda_i^{\mathrm{g}} \tag{5}$$

where λ_i^{e} and λ_i^{g} are the principal stretches related to $\boldsymbol{F}^{\mathrm{e}}$ and $\boldsymbol{F}^{\mathrm{g}}$, respectively.

Furthermore, it proves convenient to define the logarithmic strains of the above quantities as,

$$\varepsilon_i = \ln\lambda_i\,, \quad \varepsilon_i^{\mathrm{e}} = \ln\lambda_i^{\mathrm{e}}\,, \quad \varepsilon_i^{\mathrm{g}} = \ln\lambda_i^{\mathrm{g}} \tag{6}$$

and, as well, the decomposition (5) implies,

$$\varepsilon_i = \varepsilon_i^{\mathrm{e}} + \varepsilon_i^{\mathrm{g}}. \tag{7}$$

2.2 Constitutive relation for stress

Here we assume isotropy on the stress-free configuration defined by $\boldsymbol{F}^{\mathrm{g}}$. This implies that the model is invariant relative to rigid body motions with respect to the orientations on this configuration. Therefore, the strain energy function, herein denoted by ψ, could depend on the part $\boldsymbol{F}^{\mathrm{e}}$ of the deformation gradient via the elastic left Cauchy-Green tensor $\boldsymbol{b}^{\mathrm{e}} = \boldsymbol{F}^{\mathrm{e}}\boldsymbol{F}^{\mathrm{e}^T}$. The notation $(\boldsymbol{.})^{\mathrm{T}}$ is used for the transpose operator. The stress is then given by the following form of the state law,

$$\boldsymbol{\tau} = 2\frac{\partial\psi}{\partial\boldsymbol{b}^{\mathrm{e}}}\boldsymbol{b}^{\mathrm{e}} \tag{8}$$

where $\boldsymbol{\tau} = J\boldsymbol{\sigma}$ is the Kirchhoff stress tensor, $\boldsymbol{\sigma}$ being the true Cauchy stress tensor, and $J = \det[\boldsymbol{F}] > 0$ is the Jacobian of the (total) deformation gradient.

The energy function ψ can be of any form of known hyperelastic models. Here, we choose the following incompressible $N = 1$-Ogden-type model written in terms of principal stretches as,

$$\psi = \frac{2\mu}{\alpha^2}\Big(\lambda_1^{\mathrm{e}\alpha} + \lambda_2^{\mathrm{e}\alpha} + \lambda_3^{\mathrm{e}\alpha} - 3\Big) \tag{9}$$

with $J^{\mathrm{e}} \equiv \lambda_1^{\mathrm{e}}\lambda_2^{\mathrm{e}}\lambda_3^{\mathrm{e}} = 1$, μ is the shear modulus, and α is the Ogden's coefficient. Notice that by taking $\alpha = 2$, a neo-Hooke-type model is retrieved.

Next, the principal Kirchhoff stresses (the principal values of $\boldsymbol{\tau}$) are given by the corresponding form deduced from the tensorial expression (8):

$$\tau_i = \lambda_i^{\mathrm{e}}\frac{\partial\psi}{\partial\lambda_i^{\mathrm{e}}} + \varpi \tag{10}$$

where ϖ is the pressure related to the material incompressibility. It can be obtained by using the plane stress assumption $\tau_3 = 0$ as,

$$\tau_3 = \frac{2\mu}{\alpha}\lambda_3^{\mathrm{e}\alpha} + \varpi = 0 \qquad \Longrightarrow$$

$$\varpi = -\frac{2\mu}{\alpha}\lambda_3^{\mathrm{e}\alpha} \;\equiv\; -\frac{2\mu}{\alpha}(\lambda_1^{\mathrm{e}}\lambda_2^{\mathrm{e}})^{-\alpha}$$

as $\lambda_3^{\mathrm{e}} = 1/(\lambda_1^{\mathrm{e}}\lambda_2^{\mathrm{e}})$. And when substituted into equation (10), we obtain the following expression for the two remaining principal stresses:

$$\begin{aligned}\tau_\gamma &= \frac{2\mu}{\alpha}\Big(\lambda_\gamma^{\mathrm{e}\alpha} - (\lambda_1^{\mathrm{e}}\lambda_2^{\mathrm{e}})^{-\alpha}\Big)\\ &= \frac{2\mu}{\alpha}\Big(\exp\big(\alpha\varepsilon_\gamma^{\mathrm{e}}\big) - \exp\big(-\alpha(\varepsilon_1^{\mathrm{e}} + \varepsilon_2^{\mathrm{e}})\big)\Big)\end{aligned} \tag{11}$$

for $\gamma = 1, 2$. The definition $(6)_2$ has been used for the second equality, $(11)_2$.

2.3 Growth evolution equation

Concomitantly, a constitutive model for the growth evolution is to be specified. From the continuum thermodynamics point of view, the related reduced dissipation, that we denote here by $\mathcal{D}^{\mathrm{g}}$, e.g. [14], is given in terms of principal quantities as, see [16,17] for similarities with finite strain viscoelasticity,

$$\mathcal{D}^{\mathrm{g}} = \tau_i\,\dot{\varepsilon}_i^{\mathrm{g}} \geq 0. \tag{12}$$

There can exist many possible growth evolution equations that fulfil the restriction (12). Far from being arbitrary, they may be either of a simple or a complicated form. At this stage, we propose the following form:

$$\dot{\varepsilon}_\gamma^{\mathrm{g}} \;=\; \underbrace{\frac{1}{\widetilde{t}_{\mathrm{grw}}}\Big\langle\frac{\|\boldsymbol{\tau}\|}{J\sigma_{\mathrm{trs}}} - 1\Big\rangle^{+}}_{\mathcal{G}(\boldsymbol{\tau})}\;\frac{\tau_\gamma}{\|\boldsymbol{\tau}\|} \qquad \gamma = 1, 2 \tag{13}$$

where, for convenience, we have introduced the notation $\mathcal{G}(\boldsymbol{\tau})$ for the *growth* criterion. Here $\langle\boldsymbol{.}\rangle^{+}$ is the positive part function, i.e. $\langle x\rangle^{+} = \frac{1}{2}\{x + |x|\}\ \ \forall\ x$, and the notation $\|\boldsymbol{.}\|$ is used for the norm of a second-order tensor quantity.

Two essential parameters are here involved: a true stress-like growth threshold σ_{trs}, and a growth characteristic time $\widetilde{t}_{\mathrm{grw}}$. In equation (13), the growth path follows

Table 1. Parameters used for the simulation of Figure 4.

Part of the cell	Parameters
Mother cell, hyperelastic	$\mu = 40\,\text{MPa}$
Budding zone, equation (13)	$\mu = 40\,\text{MPa}$, $\widetilde{t}_{\text{grw}} = 45\,\text{min}$, $\sigma_{\text{trs}} = 1\,\text{MPa}$

the stress state through the unit tensor term $\boldsymbol{\tau}/\|\boldsymbol{\tau}\|$. Here the stress norm is given by $\|\boldsymbol{\tau}\| = \sqrt{\tau_1^2 + \tau_2^2}$.

The model can be interpreted as follows: when $\|\boldsymbol{\sigma}\| \equiv \|\boldsymbol{\tau}\|/J > \sigma_{\text{trs}}$, growth takes place. It is proportional to the stress in excess of the threshold, and its rate is controlled by the parameter $\widetilde{t}_{\text{grw}}$.

Notice further from equation (13), that the stress is here the (only) biomechanical factor that stimulates growth.

In *summary*, the present cell-wall growth model requires four mechanical parameters:

- μ, the shear modulus;
- α, the Ogden's coefficient;
- σ_{trs}, the true stress-like growth threshold;
- $\widetilde{\tau}_{\text{grw}}$, the growth characteristic time.

3 Numerical simulations and parametric studies

The proposed formulation has been implemented in an in-house finite element software through the coding of a new UMAT-like sub-routine. In this section, we provide a set of numerical simulations. We choose spherical cells with initial mid-plane diameter $D = 5$ µm and wall thickness $h = 100$ nm. These parameters are chosen based on the literature, e.g. [18,19] among others. The cell-wall is assumed homogeneous with a Young's modulus $E = 120$ MPa as found in [20,21]. This corresponds to a shear modulus $\mu = 40$ MPa because of the incompressibility. Further, we take $\alpha = 2$ for Ogden's coefficient in all the following computations in order to work with its Neo-Hookean version for the sake of simplicity.

To generate cell shape changes, we must specify:

- A budding zone at the tip of the cell. We choose for this the top zone as shown in Figure 3;
- And non-homogeneous mechanical properties. Here the bud will expand while the rest of the cell remains elastic.

Last, we must specify the turgor pressure that creates in-plane cell-wall tensions leading to the expansion. Here it is fixed to $\hat{p} = 2\,\text{atm}$, for instance as this was mentioned in [9]. Let us stress that this pressure is deformation-dependent, i.e. a follower load [22,23].

Now for the budding zone, we assign the following growth parameters:

$$\sigma_{\text{trs}} = 1\,\text{MPa}, \quad \widetilde{t}_{\text{grw}} = 45\,\text{min} \tag{14}$$

where the latter is of the order of timescales observed in budding kinetics, e.g. [10,24]. Table 1 below summarizes the parameters used for a first simulation.

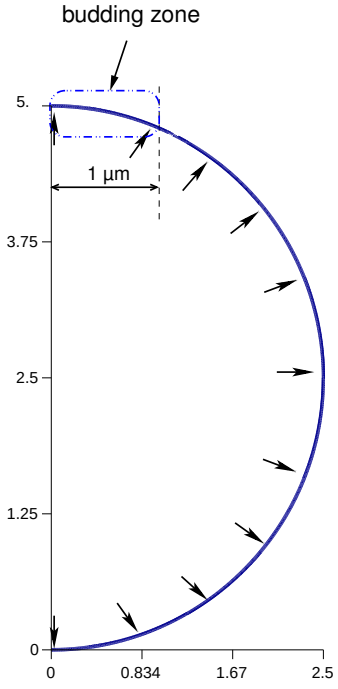

Fig. 3. Geometry of a spherical cell. The budding zone is shown at the top zone. Follower loads are used for the turgor pressure $\hat{p}$.

The axisymmetric analysis is performed with a mesh discretization using 480 uniformly distributed two-node linear shell elements (along the meridian), together with a reduced integration to avoid well-known shear locking, e.g. [12,23]. The boundary conditions only concern two nodes; the top and bottom nodes. For bottom node, the rotation and axial displacement are prescribed to zero, while for the top node, only the rotation is imposed to zero. For the time discretization, the same time step of $\Delta t = 0.2\,\text{min}$ has been used in all the simulations below.

Selected computed configurations are illustrated in Figure 4. As predicted, growth is initiated in the budding zone, Figure 4a, and continues with a large proliferation giving rise to a daughter cell, Figure 4b–c. Here, and during all the growth evolution, the mother cell remains elastic and almost undeformed after initially applying the turgor pressure.

A series of computations is next performed by fixing the growth threshold to $\sigma_{\text{trs}} = 1$ MPa, and by using different values of the growth characteristic time, here $\widetilde{t}_{\text{grw}} = 30$, 45 and 60 min. The results are shown in the form of evolutions of the internal volume V_{int} relative to the initial one V_{int_0}, see Figure 5. The first jump on the curves is due to the almost instantaneous application of the pressure $\hat{p}$, here in 0.01 min, then maintained during the whole

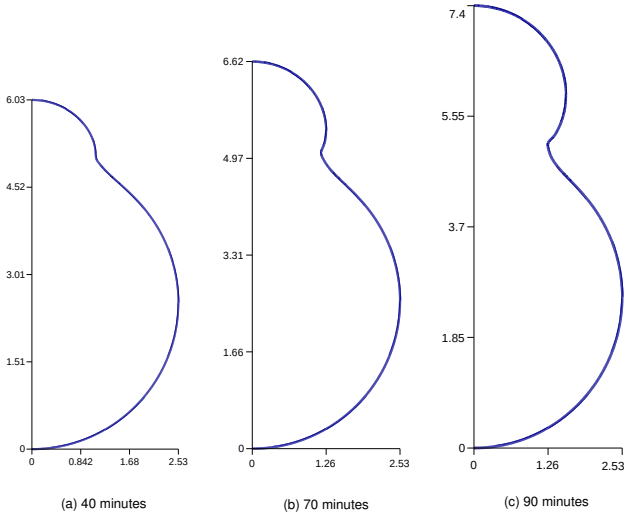

Fig. 4. Typical deformed configurations with structural shell modeling after: (a) 40 min, (b) 70 min, and (c) 90 min. The material parameters are those summarized in Table 1. The units of the graduations are scaled in (µm).

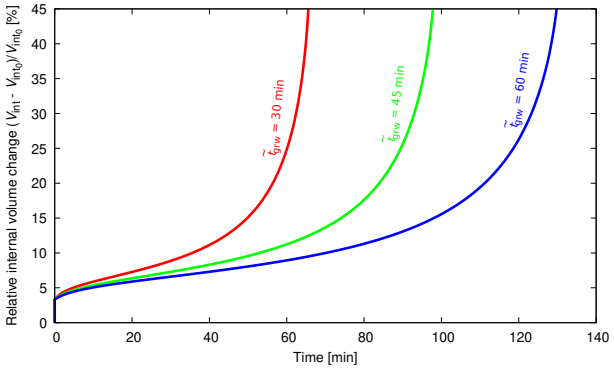

Fig. 5. Volume change due to growth for fixed stress growth threshold $\sigma_{\rm trs} = 1$ MPa, and with different growth characteristic times $\widetilde{t}_{\rm grw} = 30$, 45 and 60 min.

computations. Observe further that as the mother cell behaves elastically with low volume change, almost all the new volume is due to the growth in the daughter cell.

Likewise, a next set of computations is this time performed by fixing the characteristic time, here to $\widetilde{t}_{\rm grw} = 45$ min, and with different values of the stress threshold, here with $\sigma_{\rm trs} = 0.9$, 1, and 1.1 MPa. The results are plotted in Figure 6. One can observe that the present growth modeling framework clearly captures the influence of the stress excess with respect to the stress threshold on the growth kinetics. Notice that varying the stress threshold is equivalent to fixing this latter and varying the turgor pressure.

4 Conclusions and perspectives

The aim of this contribution was to derive a mathematical modeling framework for growth in walled cells. On the one hand, a multiplicative decomposition of the deformation gradient has been adopted within the finite strain range and, on the other hand, a growth model has been proposed. Based on the purely mechanical aspects, this latter depends on perhaps the most important parameters; a stress threshold, and a growth characteristic time. The efficiency of the proposed framework has been highlighted through a set of numerical examples with parametric studies.

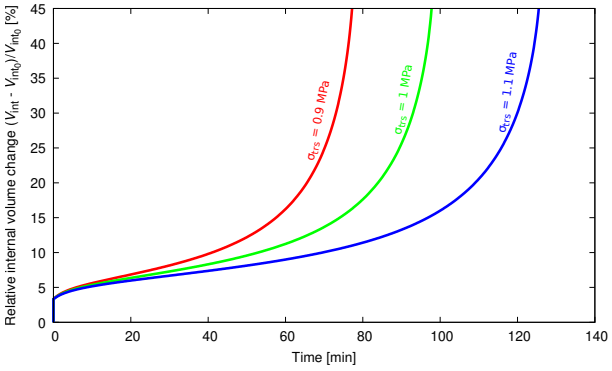

Fig. 6. Volume change due to growth for fixed growth characteristic time $\widetilde{t}_{\rm grw} = 45$ min, and with different stress thresholds $\sigma_{\rm trs} = 0.9$, 1 and 1.1 MPa.

We believe that this framework can trigger deeper research. For instance, this modeling can be enhanced by introducing further effects such as the polarization of the growth zones when coupled to more biological finds in the literature. In addition, the model is limited to the cell growth and does no include the separation of the cell daughter from the mother, which must be considered as a future research work. Moreover, an extension toward general shells will increase the field of applications, i.e. for any cell geometries.

Acknowledgments. The authors would like to thank the french ANR "Agence Nationale de la Recherche" for the financial support within the frame of Rheolife project (ANR-18-CE45-0012).

Funding

The Article Processing Charges for this article are taken in charge by the French Association of Mechanics (AFM).

References

[1] C. Lahue, A.A. Madden, R.R. Dunn, C.S. Heil, History and domestication of *Saccharomyces cerevisiae* in bread baking, Front. Genet. **11**, 1373 (2020)

[2] M. Parapouli, A. Vasileiadis, A.S. Afendra, E. Hatziloukas, *Saccharomyces cerevisiae* and its industrial applications, AIMS Microbiol. **6**, 1–31 (2020)

[3] R. Hatoum, S. Labrie, I. Fliss, Antimicrobial and probiotic properties of yeasts: from fundamental to novel applications, Front. Microbiol. **3**, 421 (2012)

[4] S. Hassan, C. Poulos, J. Bhati, S. Rangwani, Z. Khan, A. Mahmoud, T.O. Mohammed, S.R. Feldman, Saccharomyces

cerevisiae as a skin physiology, pathology, and treatment model, Dermatol. Online J. **26** (2020)
[5] S.A. Proctor, N. Minc, A. Boudaoud, F. Chang, Contributions of turgor pressure, the contractile ring, and septum assembly to forces in cytokinesis in fission yeast, Curr. Biol. **22**, 1601–1608 (2012)
[6] E. Cabib, D.H. Roh, M. Schmidt, L.B. Crotti, A. Varma, The yeast cell wall and septum as paradigms of cell growth and morphogenesis, J. Biol. Chem. **276**, 19679–19682 (2001)
[7] R. Basu, E.L. Munteanu, F. Chang, Role of turgor pressure in endocytosis in fission yeast, Mol. Biol. Cell **25**, 679–687 (2014)
[8] E.R. Rojas, K.C. Huang, Regulation of microbial growth by turgor pressure, Curr. Opin. Microbiol. **42**, 62–70 (2018)
[9] B. Goldenbogen, W. Giese, M. Hemmen, J. Uhlendorf, A. Herrmann, E. Klipp, Dynamics of cell wall elasticity pattern shapes during yeast mating Morphogenesis, Open Biol. **6**, 160136 (2016)
[10] S.P. Banavar, C. Gomez, M. Trogdon, L.R. Petzold, T.M. Yi, O. Campas, Mechanical feedback coordinates cell wall expansion and assembly in yeast mating morphogenesis, PLoS Comput. Biol. **14**, e1005940 (2018)
[11] P. Wriggers, R. Eberlein, F. Gruttman, An axisymmetrical quasi-Kirchhoff shell element for large plastic deformations, Arch. Appl. Mech. **65**, 465–477 (1995)
[12] W. Wagner, A finite element model for non-linear shells of revolution with finite rotations, Int. J. Numer. Methods Eng. **29**, 1455–1471 (1990)
[13] E. Rodriguez, A. Hoger, A. McCulloch, Stress-dependent finite growth in soft elastic tissues, J. Biomech. **27**, 455–467 (1994)
[14] B. Nedjar, On a continuum thermodynamics formulation and computational aspects of finite growth in soft tissues, Int. J. Numer. Methods Biomed. Eng. **27**, 1850–1866 (2011)
[15] J.K.E. Ortega, A.W.J. Welch, Mathematical models for expansive growth of cells with walls, Math. Model. Natural Phenomena **8**, 35–61 (2013)
[16] Z. Awada, L. Delmarre, F. Argoul, E. Harté, A. Devin, P. Argoul, B. Nedjar, Axisymmetric shell modelling of viscoelastic yeast cells in the finite strain range, in: L. Walha (Ed.), Design and Modeling of Mechanical Systems – V. CMSM 2021. Lecture Notes in Mechanical Engineering, Springer, Cham, 2023, pp. 93–102 https://doi.org/10.1007/978-3-031-14615-2-12
[17] Z. Awada, B., Nedjar, Finite viscoelastic modeling of yeast cells with an axisymmetrical shell approach, Mech. Res. Commun. **126**, 104021 (2022)
[18] F.M. Klis, C.G. de Koster, S. Brul, Cell wall-related bionumbers and bioestimates of *Saccharomyces cerevisiae* and Candida albicans, Eukaryotic Cell **13**, 2–9 (2014)
[19] A. Overbeck, I. Kampen, A. Kwade, Mechanical characterization of yeast cells: effects of growth conditions, Lett. Appl. Microbiol. **19**, 333–338 (2015)
[20] A.E. Smith, Z. Zhang, C.R. Thomas, K.E. Moxham, A.P.J. Middelberg, The mechanical properties of Saccharomyces cerevisiae, Proc. Natl. Acad. Sci. U.S.A. **97**, 9871–9874 (2000)
[21] J.D. Stenson, P. Hartley, C. Wang, C.R. Thomas, Determining the mechanical properties of yeast cell walls, Biotechnol. Progr. **27**, 505–512 (2011)
[22] B. Nedjar, A coupled BEM-FEM method for finite strain magneto-elastic boundary-value problems, Comput. Mech. **59**, 795–807 (2017)
[23] P. Wriggers, Nonlinear Finite Element Methods, Springer-Verlag, Berlin, Heidelberg, 2008
[24] B.J. Brewer, E. Chlebowicz-Sledziewska, W.L. Fangman, Cell cycle phases in unequal mother/daughter cell cycles of saccharomyces cerevisiae, *Mol. Cell. Biol.* **4**, 2529–2531 (1984)

Cite this article as: Z. Awada, B. Nedjar , Mechanical modeling of growth applied to *Saccharomyces cerevisiae* yeast cells, Mechanics & Industry **24**, 29 (2023)